

strains JH2-2 and EF228, respectively. The different molecules were added (100  $\mu$ l per well) at fixed concentrations (0, 5, 10, 50, and 100 mM) containing an inoculum of either strain at a final dilution of  $10^{-2}$  obtained from an overnight culture. The range of effective vancomycin concentrations started at 50 and 1000  $\mu$ g/ml for JH2-2 and EF228, respectively. Micro-titer plates were incubated at 37°C without agitation for 18 hours. Cell sediments were resuspended by shaking, and optical density (OD) of 600 nm was measured with an ELISA (enzyme-linked immunosorbent assay) Multiskan RC plate reader (Labsystems, Helsinki,

Finland). Bactericidal activity was determined by serially diluting ( $10^{-2}$ ,  $10^{-4}$ , and  $10^{-5}$ ) each well in BHI broth and by plating 10  $\mu$ l of each dilution on BHI agar plates. Plates were incubated for 24 hours and the number of colony-forming units per milliliter (CFU/ml) was determined.

23. S. Handwerker, M. J. Pucci, A. Kolokathis, *Antimicrob. Agents. Chemother.* **34**, 358 (1990).

24. A. E. Jacob, S. J. Hobbs, *J. Bacteriol.* **117**, 360 (1974).

25. M. H. J. Ohlmeyer *et al.*, *Proc. Natl. Acad. Sci. U.S.A.* **90**, 10922 (1993).

26. H. P. Nestler, P. A. Bartlett, W. C. Still, *J. Org. Chem.* **59**, 4723 (1994).

27. For a detailed study, see supplemental materials (21).

28. We thank W. Clark Still and A. Tomasz for providing materials and intellectual support and for critically reviewing this manuscript and C. Watson and J. Rothman for assistance and for helpful discussions. We are grateful for critical review of this manuscript by A. Labigne, H. de Reuse, C. Le-Bouguenec, T. Muir, N. Rosen, and S. Shuman. Supported by NIH. I.G.B. was supported by a fellowship from the Praxis XXI program (BD/2379/94, Portugal).

1 March 2001; accepted 3 July 2001

## Enhanced Neurofibrillary Degeneration in Transgenic Mice Expressing Mutant Tau and APP

Jada Lewis,\* Dennis W. Dickson,\* Wen-Lang Lin, Louise Chisholm, Anthony Corral, Graham Jones, Shu-Hui Yen, Naruhiko Sahara, Lisa Skipper, Debra Yager, Chris Eckman, John Hardy, Mike Hutton,† Eileen McGowan

JNPL3 transgenic mice expressing a mutant tau protein, which develop neurofibrillary tangles and progressive motor disturbance, were crossed with Tg2576 transgenic mice expressing mutant  $\beta$ -amyloid precursor protein (APP), thus modulating the APP-A $\beta$  ( $\beta$ -amyloid peptide) environment. The resulting double mutant (tau/APP) progeny and the Tg2576 parental strain developed A $\beta$  deposits at the same age; however, relative to JNPL3 mice, the double mutants exhibited neurofibrillary tangle pathology that was substantially enhanced in the limbic system and olfactory cortex. These results indicate that either APP or A $\beta$  influences the formation of neurofibrillary tangles. The interaction between A $\beta$  and tau pathologies in these mice supports the hypothesis that a similar interaction occurs in Alzheimer's disease.

Alzheimer's disease (AD) is pathologically characterized by senile plaques, largely composed of extracellular deposits of A $\beta$  peptide, and neurofibrillary tangles (NFTs), composed of intracellular filamentous aggregates of hyperphosphorylated tau protein. Since the initial molecular characterizations of these lesions (1–3), there has been controversy over how these lesions and their constituent molecules are pathogenically related to each other and to the neuronal and synaptic losses that characterize the disease (4–6). A key part of this debate has been the observation that the pathogenic mutations that underlie the autosomal dominant forms of the disease—mutations in APP or in the presenilins PS-1 and PS-2 (7–9)—lead to increased production of the A $\beta$ 42 peptide in tissues from affected individuals (10), in transfected cells (11–13), and in transgenic animals (12, 14–18). Some transgenic mouse models for AD, overexpressing mutant human APP alone or

with mutant PS-1, develop senile plaques; however, these mice lack NFTs and exhibit little neuronal loss (14–18). This has limited their use as models of disease and fueled the notion that senile plaques and NFTs are generated by independent processes.

Neurofibrillary pathology is also a feature of other neurodegenerative diseases, including FTDP-17 (frontotemporal dementia and Parkinsonism linked to chromosome 17). Mutations in the *tau* gene underlie FTDP-17, hence tau dysfunction is sufficient to cause neurodegeneration (19). Furthermore, JNPL3 transgenic mice with the Pro<sup>301</sup>  $\rightarrow$  Leu (P301L) tau mutation develop NFTs in the basal telencephalon, diencephalon, brainstem, and spinal cord, along with neuronal loss that is most evident in the spinal cord, especially in the anterior horn (20).

The production of these mutant tau transgenic mice provided the opportunity to test experimentally whether the distribution or timing of neurofibrillary pathology is influenced by the pathogenic mutations that cause AD. Therefore, we crossed Tg2576 transgenic mice expressing the APPsw mutation (Lys<sup>670</sup>  $\rightarrow$  Asn, Met<sup>671</sup>  $\rightarrow$  Leu) (15, 21, 22) with JNPL3 transgenic mice expressing mu-

tant P301L four-repeat tau (20) and compared the pathology of the crossed mice with each of their parental lines (23).

Previous studies have shown that Tg2576 mice have markedly elevated A $\beta$  levels at an early age and develop extracellular A $\beta$  deposits in the cortex and hippocampus by 9 to 12 months of age (15). Hemizygous JNPL3 mice develop progressive motor and behavioral abnormalities with robust neurofibrillary pathology and neuronal loss in the spinal cord as early as 6.5 months (20). In JNPL3 animals, NFTs are primarily located in the spinal cord and the hindbrain, with fewer NFTs in the midbrain, amygdala, and hypothalamus (20). Pretangles, which are neurons that have abnormal expression of phospho-tau epitopes, are found in greater numbers and have a wider distribution throughout the spinal cord and brain, most notably in limbic structures such as the hippocampus and amygdala. Neither pretangles nor NFTs are detected in the basal ganglia of JNPL3 mice.

We examined the brains and spinal cords of Tg2576  $\times$  JNPL3 progeny at 2.5 to 3.5 months, 6 to 7 months, and 8.5 to 15 months of age (24–29). These progeny included double mutant tau (P301L)–mutant APP (APPsw) (hereafter termed TAPP mice), mutant tau (JNPL3), mutant APP (Tg2576), and nontransgenic animals. TAPP mice had amyloid plaques similar in number and distribution to those of comparably aged Tg2576 mice. Plaques were detected as early as 6 months of age but became numerous only in older TAPP and Tg2576 mice (8.5 to 15 months) in the olfactory cortex, cingulate gyrus, amygdala, entorhinal cortex, and hippocampus (Fig. 1) (30). NFTs were morphologically similar in TAPP and JNPL3 mice and appeared in the spinal cord and pons as early as 3 months of age, but were consistently present and numerous only in older animals (Figs. 2 and 3). Some of the NFTs were fluorescent when stained with thioflavin-S, and all were intensely positive for Gallyas silver stain and immunoreactive with a panel of antibodies to tau protein, including antibodies to phosphorylation-dependent and conformational epitopes (24–28) (Fig. 1). Ultrastructurally, NFTs in the TAPP mice were also similar to those in JNPL3 mice and were composed of straight filaments, 17 to 22 nm

Birdsall Building, Mayo Clinic Jacksonville, 4500 San Pablo Road, Jacksonville, FL 32224, USA.

\*These authors contributed equally to this report.  
†To whom correspondence should be addressed. E-mail: hutton.michael@mayo.edu

## REPORTS

in diameter, that sometimes formed complex arrangements with a herringbone appearance similar to those described in Pick's disease (Fig. 1) (31). Tau filaments occupied a large proportion of the cell volume in neurons with NFTs, displacing the nucleus and cytoplasmic organelles and compressing the Golgi apparatus.

Although NFTs were morphologically similar in the TAPP and JNPL3 (mutant tau) mice, older female TAPP mice (9 to 11 months) had a marked increase in NFTs in limbic areas, most notably the olfactory cortex, entorhinal cortex, and amygdala. This enhanced neurofibrillary degeneration occurred as early as 6 months of age. The density of NFTs in these regions in female TAPP mice (9 to 11 months) was greater than in female JNPL3 littermates by a factor of more than 7 ( $P < 0.012$  to  $P < 0.0009$ ) (Figs. 2 and 3). NFTs were also detected in the subiculum, hippocampus, and occasionally isocortex in the TAPP animals, areas that rarely or never had NFTs in JNPL3 mice. The number and distribution of pretangles was also increased in female TAPP mice (9 to 11 months) in limbic areas and cerebral cortex. In contrast, subcortical neurofibrillary pathology was similar in female TAPP and JNPL3 mice, with no increase in density of either NFTs or pretangles in the diencephalon, hindbrain, or spinal cord (Fig. 3). NFTs and pretangles were not observed in the basal ganglia in TAPP mice. In limbic areas with the most NFTs, there was a concomitant increase in astrogliosis (Fig. 2) in TAPP mice. In contrast, in the ventral diencephalon, hindbrain, and spinal cord of JNPL3 and TAPP mice, gliosis was equally severe. Enhanced neurofibrillary pathology in female TAPP mice (9 to 11 months) in limbic regions is of interest because these are the areas in which A $\beta$  pathology first develops in Tg2576 mice (15).

However, even in areas vulnerable to both types of lesions (such as the entorhinal cortex), NFTs were not typically increased in the immediate vicinity of amyloid deposits. The fact that amyloid plaques were not generally surrounded by tangle-bearing neurons suggests that either a high-A $\beta$  environment or APP dysfunction, but not necessarily the formation of mature amyloid deposits, is responsible for the modulation and enhancement of the tau phenotype in the TAPP mice. Interestingly, male TAPP mice did not develop similar enhanced NFT pathology in limbic regions (Fig. 3). This likely reflects sex differences in the development of NFT pathology previously observed in the JNPL3 line; female mice develop NFT pathology significantly earlier than do males (32). However, the difference between female and male TAPP mice could also be caused by significant sex differences in amyloid burden pre-

viously noted in older Tg2576 mice (33) or could reflect hormonal changes in aging female TAPP mice. The latter possibility is interesting given the higher incidence of AD in women (34–36).

The morphology, distribution, and density of the amyloid plaques were similar in TAPP mice and age-matched Tg2576 mice (Fig. 1) (30). The amyloid deposits were immunoreactive for both A $\beta$ 40 and A $\beta$ 42 (30). In addition, dystrophic neurites immunoreactive for APP were associated with the senile plaques in both TAPP and Tg2576 mice (30). Some of the plaques had neurites that were immunoreactive with phospho-tau antibodies, but plaque-associated neurites were not

detected with antibodies specific to conformational tau epitopes, such as Alz50 and MC1, or antibodies specific to NFTs, such as Ab39 (Fig. 1) (30). To date, we have not identified plaque-associated dystrophic neurites containing tau-immunoreactive filamentous structures at the ultrastructural level.

Brain A $\beta$ 1-40 and A $\beta$ 1-42 were measured in hemibrains from 9- to 11-month-old TAPP mice and from Tg2576 littermates (15, 37–39). A $\beta$ 40 and A $\beta$ 42 levels were similar in the brains of TAPP mice (553 pmol/g and 352 pmol/g, respectively) and Tg2576 littermates (560 pmol/g and 421 pmol/g, respectively), consistent with the absence of a detectable difference in A $\beta$  plaque burden in

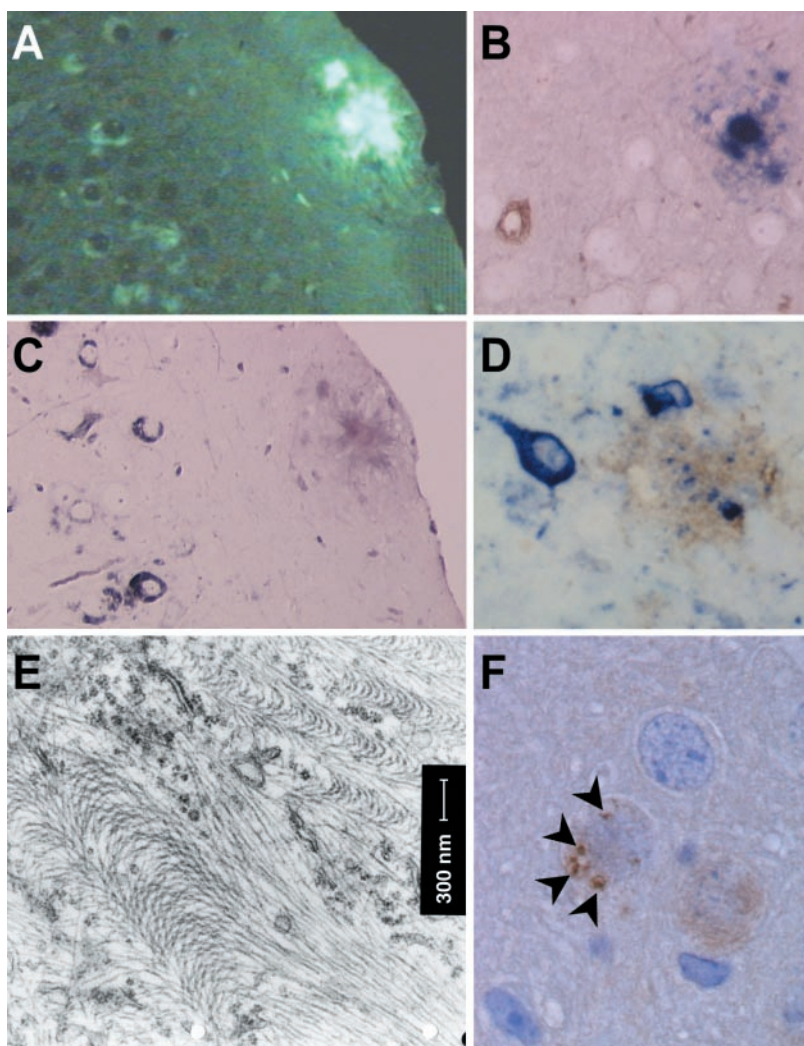


**Fig. 1.** NFTs and amyloid plaques in TAPP mice. (A and C) Adjacent sections of entorhinal cortex viewed with thioflavin-S fluorescent microscopy (A) or Gallyas silver stain (C) show both amyloid plaques and NFTs in female TAPP mice. (B and D) Amyloid plaques are immunostained with a rabbit antibody to A $\beta$ 42 and double-immunostained with mouse antibodies to tau. In (B), a tangle-specific mAb (Ab39) identifies a NFT (left) but no neurites in the plaque. In (D), double staining of a diffuse amyloid deposit in the frontal cortex shows local phospho-tau (PG5) immunoreactivity in neurons and neuronal cell processes associated with the plaque. (E) Ultrastructural studies of entorhinal NFTs reveal aggregates of criss-crossing straight filaments that are about 20 nm in diameter. (F) Granulovacuolar bodies (arrowheads) are detected in neurons in the amygdala, entorhinal cortex, and subiculum with phospho-tau antibodies (TG3). Mice were aged 9.5 to 10.5 months. Magnifications: (A) and (C), 200 $\times$ ; (B), (D), and (F), 400 $\times$ .

## REPORTS

the TAPP mice compared with Tg2576 mice at the same age. A larger series of animals, however, will be needed to determine whether there are significant differences in the initial levels of A $\beta$  in young TAPP mice and in the rate of A $\beta$  deposition as the mice age.

Levels of total soluble endogenous and transgenic tau protein (40) and *tau* mRNA (41) were similar in TAPP and JNPL3 brains (30). In addition, in situ hybridization analysis showed no difference in *tau* transgene expression pattern between TAPP and JNPL3 mice. These data indicate that there was no global or region-specific increase in tau expression that could explain the enhanced neurofibrillary pathology in the TAPP mice.

Sarkosyl-insoluble tau extracted from both TAPP and JNPL3 mice contained a major hyperphosphorylated species migrating at 64 kD (Fig. 3) that increased as a propor-

tion of the total insoluble tau with age. Dephosphorylation studies in JNPL3 mice and in humans with AD and FTDP-17 have shown that the 64-kD band contains hyperphosphorylated tau of the same isoform expressed by the tau transgene (20). The 64-kD insoluble tau species (42, 43) extracted from the cortex/limbic fraction (fraction 1) of the mouse brain was increased in female TAPP mice (9.5 to 11 months) relative to female JNPL3 mice, but not in the fraction (fraction 2) containing the subcortical regions, brainstem, and cerebellum (Fig. 3). This elevation of 64-kD insoluble tau in the female TAPP animals (9.5 to 11 months) correlates with histopathologic evidence of enhanced neurofibrillary pathology in the limbic system of the oldest female TAPP mice. At earlier time points (3 and 6 months), insoluble tau could be detected in both fractions in TAPP and JNPL3 mice;

however, enhanced insoluble tau in the cortex/limbic fraction was not observed in TAPP mice. This correlates with the observation that significant increases in limbic NFT pathology are detected only after 9 months in female TAPP mice (Fig. 3).

In addition to increased NFTs, granulovacuolar degeneration was observed in neurons in the amygdala, entorhinal cortex, and subiculum in female TAPP mice (Fig. 1). Granulovacuolar degeneration was characterized by optically clear vacuoles with dense cores that contained phosphorylated epitopes recognized by TG3 and MPM-2 monoclonal antibodies (mAbs) (44, 45). In contrast, only neurons in the amygdala of JNPL3 mice showed rare granulovacuolar degeneration.

TAPP mice developed motor disturbances similar to their JNPL3 littermates, with identical range in age of onset, including progressive hindlimb weakness, hunched posture, eye irritations, reduced vocalization, and decreased grooming (20). The motor phenotype is most likely associated with the spinal cord and neuromuscular pathology that was similar in both TAPP and JNPL3 mice.

Our results reveal an interaction between APP or A $\beta$  and tau (46) that leads to increased NFT formation and distribution in regions of brain vulnerable to these lesions. Most important, the findings for TAPP mice show that improved rodent models of AD are possible using an APP-tau cross-breeding strategy. These models should allow therapies to be developed and tested that address not only amyloid deposition but also NFT formation and neuronal loss, features of AD that previous transgenic mice have failed to recapitulate.

*Note added in proof:* Götz *et al.* (47) injected A $\beta$ 42 fibrils into the brains of P301L mutant tau transgenic mice and noted a factor of 5 increase in the numbers of NFTs in the amygdala from where neurons project to the injection sites. These data are consistent with our own observations in TAPP mice and further support the hypothesis that there is an interaction between the A $\beta$  and tau pathologies in AD.

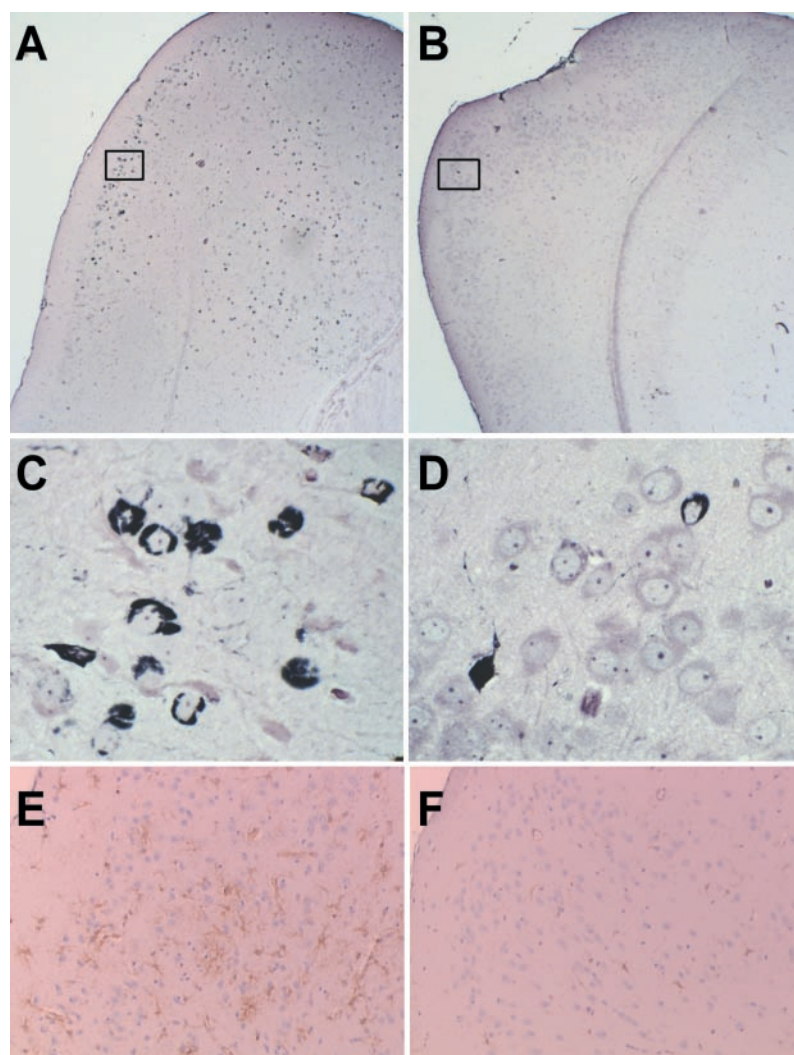


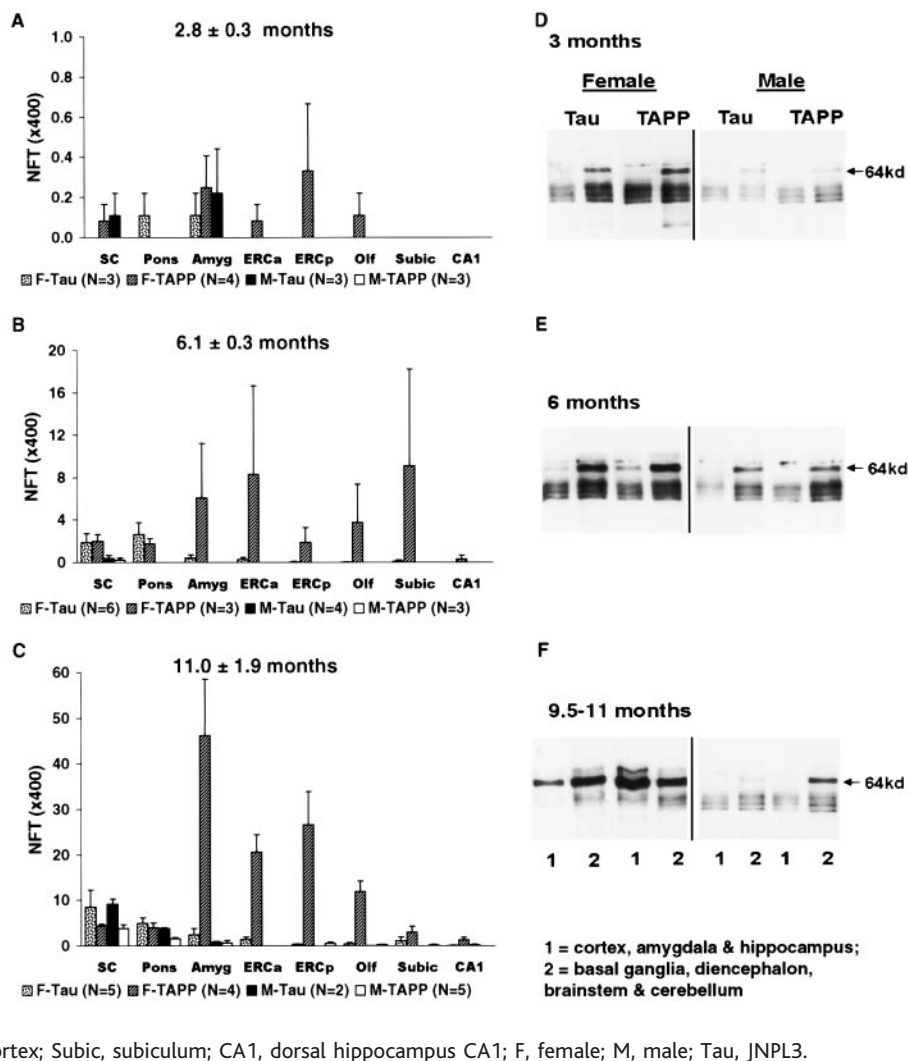
**Fig. 2.** Enhanced limbic neurofibrillary pathology in TAPP mice. Gallyas silver-stained preparations show enhanced neurofibrillary degeneration in the amygdala and adjacent entorhinal cortex of female TAPP mice (A and C) relative to age-matched JNPL3 mice (B and D); boxes in (A) and (B) correspond to regions in (C) and (D), respectively. Note the pyknosis of non-tangle-bearing neurons in (C). Immunostaining for GFAP also reveals gliosis in female TAPP mice (E) that is minimal in female JNPL3 mice (F). Sections are from 9-month-old mice. Magnifications: (A) and (B), 40 $\times$ ; (C) and (D), 400 $\times$ ; (E) and (F), 200 $\times$ .

### References and Notes

- G. G. Glenner, C. W. Wong, *Biochem. Biophys. Res. Commun.* **122**, 131 (1984).
- C. L. Masters *et al.*, *EMBO J.* **4**, 2757 (1985).
- C. M. Wischik *et al.*, *Proc. Natl. Acad. Sci. U.S.A.* **85**, 4506 (1988).
- J. Hardy, D. Allsop, *Trends Pharmacol. Sci.* **12**, 383 (1991).
- D. Selkoe, *J. Neuropathol. Exp. Neurol.* **53**, 438 (1994).
- A. D. Roses, *J. Neuropathol. Exp. Neurol.* **53**, 429 (1994).
- A. Goate *et al.*, *Nature* **349**, 704 (1991).
- R. Sherrington *et al.*, *Nature* **375**, 754 (1995).
- E. Levy-Lahad *et al.*, *Science* **269**, 973 (1995).
- D. Scheuner *et al.*, *Nature Med.* **2**, 864 (1996).
- D. R. Borchelt *et al.*, *Neuron* **17**, 1005 (1996).
- M. Citron *et al.*, *Nature Med.* **3**, 67 (1997).
- N. D. Mehta *et al.*, *Ann. Neurol.* **43**, 256 (1998).

## REPORTS

**Fig. 3.** Analysis of neurofibrillary pathology and sarkosyl-insoluble tau. (A to C) NFTs were counted in eight neuroanatomical regions (average of three fields) on Gallyas-stained brain sections (5  $\mu$ m) of male and female TAPP and JNPL3 mice ranging in age from 2.5 to 15 months. Occasional NFTs were detected at 3 months of age in TAPP and JNPL3 mice in brain and spinal cord, with sparse NFTs noted in cerebral areas in female TAPP but not JNPL3 mice (A). By 6 to 7 months of age, TAPP mice had consistent NFTs in limbic areas, but in JNPL3 mice NFTs were largely restricted to spinal cord and pons (B); however, there were no statistically significant differences at this age range. There were statistically significant increases ( $P < 0.012$  to  $P < 0.0009$ ) in NFTs in the amygdala, anterior and posterior entorhinal cortex, olfactory cortex, subiculum, and dorsal hippocampus CA1 in the oldest female TAPP mice relative to age-matched female JNPL3 mice (C); the oldest female TAPP mice had significantly more NFTs than the oldest male TAPP mice (ranging from  $P < 0.012$  to  $P < 0.0005$ ) in all regions except the spinal cord and pons. (D to F) Sarkosyl-insoluble tau was immunoblotted with a human-specific tau antibody, E1. JNPL3 and TAPP mice had sarkosyl-insoluble tau, including a 64-kD hyperphosphorylated species, as early as 3 months of age (D). At all ages, female JNPL3 and TAPP mice had more insoluble tau than did male mice. In the younger age groups [(D) and (E)], a greater amount of insoluble tau was extracted from brain fraction 2 (basal ganglia, diencephalon, brainstem, and cerebellum) than from fraction 1 (cortex, amygdala, and hippocampus). In contrast, 9.5- to 11-month-old female TAPP mice had more sarkosyl-insoluble tau in fraction 1 than did female JNPL3 mice, consistent with the enhanced neurofibrillary pathology in these areas (F). Abbreviations: SC, spinal cord; Amyg, amygdala; ERCa, anterior entorhinal cortex; ERCp, posterior entorhinal cortex; Olf, olfactory cortex; Subic, subiculum; CA1, dorsal hippocampus CA1; F, female; M, male; Tau, JNPL3.



14. D. Games *et al.*, *Nature* **373**, 523 (1995).
15. K. Hsiao *et al.*, *Science* **274**, 99 (1996).
16. K. Duff *et al.*, *Nature* **383**, 710 (1996).
17. D. R. Borchelt *et al.*, *Neuron* **19**, 939 (1997).
18. L. Holcomb *et al.*, *Nature Med.* **4**, 97 (1998).
19. J. Lewis, M. Hutton, *Neurosci. News* **3**, 63 (2000).
20. J. Lewis *et al.*, *Nature Genet.* **25**, 402 (2000).
21. M.ullan *et al.*, *Nature Genet.* **1**, 345 (1992).
22. L. Lannfelt *et al.*, *Neurosci. Lett.* **168**, 254 (1994).
23. Double mutant mice were generated by crossing hemizygote Tg2576  $\times$  hemizygote JNPL3. Mice were maintained on a SW/DBA2/C57B6 background. Mice were genotyped for the tau transgene by polymerase chain reaction (PCR) between exons 1 and 5 of the human tau cDNA against an internal PS-2 control PCR. Mice were genotyped for the APP transgene by PCR between exon 15 of the human APP gene and the hamster prion protein promoter against an internal  $\beta$ -actin control PCR.
24. For pathological studies, immersion-fixed (4% paraformaldehyde or 10% formalin) paraffin-embedded brain sections (5 to 7  $\mu$ m thick) were immunostained with an avidin biotin peroxidase (ABC) method (Vector Labs, Burlingame, CA) and the following tau antibodies: Ab39 (Yen, 1:10); Alz50 (Davies, 1:10); PHF1 (Davies, 1:100); TG3 (Davies, 1:10); CP3 (Davies, 1:100); CP13 (Davies, 1:100); PG5 (Davies, 1:100); E-1 (Yen, 1:1000); RT97 (Anderton, 1:100); AT180 (Innogenetics, 1:100); a polyclonal antibody to ubiquitin, UH19 (Ksiazak-Reding, 1:500); a polyclonal antibody to  $\alpha$ B-crystallin (Novacastra, 1:250); an antibody to mitotic phosphoepitopes, MPM-2 (Accurate Chem-

icals & Scientific Products, 1:200); glial fibrillary acidic protein (GFAP) mAb (Biogenex, 1:100); and APP mAb 22C11 (Boehringer Mannheim, 1:20). Double immunohistochemical methods were used to evaluate senile plaques in TAPP and Tg2576 mice. In some experiments, sections that had been immunostained with peroxidase methods for dystrophic neurites were counterstained with thioflavin-S. In other experiments, double staining was performed with species- and isotype-specific secondary antibodies applied as cocktails after incubating in cocktails containing two primary antibodies in various combinations. The secondary antibodies were labeled with alkaline phosphatase or horseradish peroxidase. The chromogens were developed sequentially. In all experiments, the labeled secondary antibodies were reversed and formalin-fixed, paraffin-embedded sections of human AD brain were run concurrently as positive controls. Paraffin-embedded sections were used for histochemical stains (hematoxylin and eosin), thioflavin-S, Congo Red, and Braak's modification of the Gallyas silver stain. NFTs were counted in Gallyas-stained sections of brain and spinal cord in eight neuroanatomic regions with an Olympus BX50 microscope using a 40 $\times$  objective lens ( $\times$ 400). In each region, counts were made in three nonoverlapping fields chosen to include the highest lesion density, and the average NFT count was calculated. Amyloid plaques were counted in thioflavin-S-stained sections of brain in five neuroanatomic regions with an Olympus BH2 fluorescent microscope using a 10 $\times$  objective lens ( $\times$ 100). A

single low-power field was chosen from each region to include the maximum lesion density. Statistical comparisons for lesion density and of male-female differences in TAPP and JNPL3 were performed with the Student *t* test and Mann-Whitney rank sum using SigmaStat version 2; a significance level of  $P < 0.05$  was used.

25. The following antibodies were used to stain NFTs in TAPP mice. Conformational tau epitopes: Alz50, MC-1, and Ab39. Phosphorylated tau epitopes: RT97 (phospho-46), CP13 (phospho-202/205), CP3 (phospho-214), AT180 (phospho-231/235), TG3 (phospho-231/235), PHF-1 (phospho-396/404), and PG5 (phospho-409). Other antibodies: E1 (human-specific tau exon 1 polyclonal antibody) and MPM-2 (mitotic phosphoepitope).
26. G. A. Jicha, R. Bowser, I. G. Kazam, P. Davies, *J. Neurosci.* **18**, 128 (1997).
27. G. A. Jicha, *J. Neurosci.* **19**, 7486 (1999).
28. M. DeTure, L.-W. Ko, C. Easson, M. Hutton, S.-H. Yen, in *Alzheimer's Disease: Advances in Etiology, Pathogenesis and Therapeutics*, K. Iqbal, S. S. Sisodia, B. Winblad, Eds. (Wiley, New York, 2001), pp. 651-660.
29. For electron microscopy, brain and spinal cord were dissected and immersion-fixed in paraformaldehyde; thin sections of briefly fixed brain (4% paraformaldehyde) were trimmed to 1-mm<sup>3</sup> pieces, fixed in 2.5% glutaraldehyde-0.1 M cacodylate buffer (pH 7.4), post-fixed in 1% osmium tetroxide, and dehydrated in a graded series of alcohols and propylene oxide before infiltration and embedding in epoxy resin (Poly Bed 812; Polysciences, Warrington, PA). Ultrathin sections were stained with uranyl acetate

and lead citrate for transmission electron microscopy using a Philips 208S.

30. For supplemental data, see Science Online ([www.sciencemag.org/cgi/content/full/293/5534/1487/DC1](http://www.sciencemag.org/cgi/content/full/293/5534/1487/DC1)).

31. J. Mikol, S. Brion, L. Guicharnaud, O. Waks, *Acta Neuropathol.* **49**, 57 (1980).

32. Studies of the JNPL3 mice have indicated that there are sex differences in the development of NFT pathology. Female mice have higher tau expression in the central nervous system relative to males (in situ hybridization, Northern, and Western analysis) and develop tau pathology and motor disturbance at an earlier age. Similar higher levels of tau expression in female mice have also been observed in a second transgenic mouse line expressing the longest 4R tau isoform with the P301L mutation.

33. M. J. Callahan *et al.*, *Am. J. Pathol.* **158**, 1173 (2001).

34. A. F. Jorm, A. E. Korten, A. S. Henderson, *Acta Psychiatr. Scand.* **76**, 465 (1987).

35. W. A. Rocca *et al.*, *Ann. Neurol.* **30**, 381 (1991).

36. C. H. Kawas, R. Katzman, in *Alzheimer Disease*, R. D. Terry, R. Katzman, K. L. Bick, S. Sisodia, Eds. (Lippincott Williams & Wilkins, Philadelphia, ed. 2, 1999), pp. 95–116.

37. For  $\beta$  measurements, one hemisphere was dounce-homogenized in 70% formic acid and centrifuged at 100,000g for 1 hour; the resulting supernatant was neutralized by a 1:20 dilution in 1 M tris base followed by dilution in buffer EC (0.02 M  $\text{Na}_2\text{HPO}_4$ , 0.002 M EDTA, 0.4 M NaCl, 0.2% BSA, 0.05% CHAPS, 0.04% BlockAce, 0.05%  $\text{NaN}_3$ , pH 7.0).  $\beta$  values were determined by sandwich enzyme-linked immunosorbent assay (ELISA) using the BAN50/BA27 and BAN50/BC05 ELISA systems for  $\beta$ 40 and  $\beta$ 42, respectively. The values presented were calculated by determining the amount of  $\beta$  detected relative to synthetic human  $\beta$ 1-40 and  $\beta$ 1-42 and converting to pmol per gram of wet weight of brain.

38. S. A. Gravina *et al.*, *J. Biol. Chem.* **270**, 10713 (1995).

39. S. J. Haugabook *et al.*, *FASEB J.* **15**, 16 (2001).

40. For total soluble tau Western blots, mouse brains were harvested and snap-frozen; immunoblotting was performed by homogenizing half of a mouse brain in buffer containing protease inhibitor (1 mM phenylmethylsulfonyl fluoride, 20  $\mu$ M aprotinin, 10  $\mu$ M leupeptin, and 1 mM EGTA) and phosphatase inhibitor (5 mM sodium pyrophosphate, 30 mM  $\beta$ -glycerophosphate, and 30 mM sodium fluoride). Homogenates were dissolved in sample buffer and run on a 10% SDS-polyacrylamide gel electrophoresis (PAGE) gel, transferred to nitrocellulose, and stained with a human tau-specific antibody, E1, and an antibody that recognizes mouse and human tau (WKS45). Equivalent sample loading was determined by protein assay and confirmed by probing the tau blots with an antibody to  $\beta$ -tubulin (Sigma). The antibody, E1, was raised to amino acid residues 19 to 33 of human tau. WKS45 is a polyclonal antibody that recognizes mouse and human tau (amino acids 258 to 266). Quantitation of Western blots was performed by image analysis using MCID software (Research System Inc.). The ratio of tau to tubulin in different samples was compared.

41. For Northern analysis, total RNA was extracted from crushed whole mouse brains using Trizol (Life Technologies); RNA (15  $\mu$ g) was electrophoresed on a denaturing gel, transferred overnight onto a nylon membrane (Hybond-N<sup>+</sup>, Amersham Life Science), and cross-linked. An oligomer designed to exon 11 of human/mouse tau (5'-AGATTTTACTTCCACCTGGCCACTCTG-3') was used to assess transgenic mRNA levels. Probes were 3' end-labeled with [ $\alpha$ -<sup>32</sup>P]deoxyadenosine triphosphate. The membrane was hybridized in buffer [containing 4 $\times$  SSC, 1 $\times$  Denhardt's solution, 50% (w/v) deionized formamide, 10% (w/v) dextran sulfate, and herring sperm DNA (200 mg/ $\mu$ l)] with the labeled probe overnight at 42°C. The membrane was washed stringently (1 $\times$  SSC/0.1% SDS at 55°C) and exposed to BioMax maximum-sensitivity film (Kodak) at -80°C and Amersham Phosphor Imaging Screens for 1 to 2 days. Band quantification was performed using a Storm Phosphor scanner and ImageQuant software (Molecular Dynamics). Membranes were stripped and reprobed with a <sup>32</sup>P-labeled histone cDNA probe to assess loading.

42. For analysis of sarkosyl-insoluble tau, brain tissue (sectioned into cortex-limbic and subcortical-basal ganglia-cerebellum fractions) was homogenized in tris-buffered saline (TBS); a small sample was removed for the analysis of total tau, and the remainder was centrifuged at 100,000g for 1 hour at 4°C. The pellet was homogenized in 0.8 M NaCl and 10% sucrose in TBS. After centrifugation at 150,000g for 15 min, the supernatant was brought to 1% sarkosyl and incubated at 37°C for 1 hour. The mixture was then centrifuged at 150,000g for 30 min and the precipitate was collected as the sarkosyl-insoluble fraction. Equal amounts (v/w) of insoluble tau preparations were analyzed by SDS-PAGE and Western blotting using an antibody specific to human tau (E1, amino acids 19 to 33) and one that recognizes both human and mouse tau (WKS45, amino acids 258 to 266). Hyperphosphorylated tau was detected with PHF-1 (phospho-396/404).

43. S. G. Greenberg, P. Davies, *Proc. Natl. Acad. Sci. U.S.A.* **87**, 5827 (1990).

44. D. W. Dickson *et al.*, *Acta Neuropathol.* **85**, 463 (1993).

45. I. Vincent, J. H. Zheng, D. W. Dickson, Y. Kress, P. Davies, *Neurobiol. Aging* **19**, 287 (1998).

46. J. Hardy, K. Duff, K. Gwinn-Hardy, J. Perez-Tur, M. Hutton, *Nature Neurosci.* **1**, 355 (1998).

47. J. Götz, F. Chen, J. van Dorpe, R. M. Nitsch, *Science* **293**, 1491 (2001).

48. We thank P. Davies (Albert Einstein College of Medicine) for antibodies, V. Philips and L. Rousseau for histopathology, and D. Forste, E. Kirkham, C. Ortega, and F. Conkle for mouse maintenance. Supported by the National Institute on Aging (PO1 grant to D.W.D., S.-H.Y., J.H., M.H.), National Institute of Neurological Diseases and Stroke (M.H.), Mayo Foundation, Smith Scholar Program (J.L., C.E.), John Douglas French Alzheimer's Foundation (J.L.), MetLife Foundation (D.W.D., M.H.), and Mayo Clinic Alzheimer's Disease Research Center (E.M.).

11 December 2000; accepted 14 June 2001

## Formation of Neurofibrillary Tangles in P301L Tau Transgenic Mice Induced by $\text{A}\beta$ 42 Fibrils

J. Götz,<sup>1\*</sup>† F. Chen,<sup>1\*</sup> J. van Dorpe,<sup>2</sup> R. M. Nitsch<sup>1‡</sup>

$\beta$ -Amyloid plaques and neurofibrillary tangles (NFTs) are the defining neuropathological hallmarks of Alzheimer's disease, but their pathophysiological relation is unclear. Injection of  $\beta$ -amyloid  $\text{A}\beta$ <sub>42</sub> fibrils into the brains of P301L mutant tau transgenic mice caused fivefold increases in the numbers of NFTs in cell bodies within the amygdala from where neurons project to the injection sites. Gallyas silver impregnation identified NFTs that contained tau phosphorylated at serine 212/threonine 214 and serine 422. NFTs were composed of twisted filaments and occurred in 6-month-old mice as early as 18 days after  $\text{A}\beta$ <sub>42</sub> injections. Our data support the hypothesis that  $\text{A}\beta$ <sub>42</sub> fibrils can accelerate NFT formation in vivo.

Transgenic mice that express P301L mutant human tau form abnormal tau-containing filaments in brains (1, 2). These filaments have striking similarities with the NFTs of several human neurodegenerative diseases, including Alzheimer's disease (AD) and frontotemporal dementia with parkinsonism linked to chromosome 17 (FTDP-17), but their numbers are considerably lower than these commonly found in human disease (3). To determine whether  $\beta$ -amyloid can accelerate NFT formation, we injected synthetic  $\text{A}\beta$ <sub>42</sub> fibrils into the somato-

sensory cortex and the hippocampus of 5- to 6-month-old P301L tau transgenic mice (4) and nontransgenic littermates (5–7). For the control peptide, we used the reversed sequence,  $\text{A}\beta$ <sub>42-1</sub>, derived from the identical source (6).  $\text{A}\beta$ <sub>42</sub> fibrils were generated by incubation at 37°C with shaking and were confirmed by electron microscopy (Fig. 1, A and B) (5, 6).  $\text{A}\beta$ <sub>42</sub> fibrils were stable in vivo in both P301L transgenic and wild-type control mice and were readily detectable at least until 45 days after the injections (Fig. 1C). As expected, brain amyloid deposits were accompanied by reactive astrogliosis at both the injection sites (Fig. 1D) and the amygdala (Fig. 1E) (8); these were seen in both  $\text{A}\beta$ <sub>42</sub>- and in control-injected transgenic mice and persisted for at least 45 days after injection. This reaction may be related to the fact that neurons in the amygdala project to the injection sites, as shown by retrograde transport of Texas red-conjugated dextran from the injection site in the somatosensory cortex to cell bodies in the amygdala (Fig. 1F) (8).

Eighteen days after the injections of  $\text{A}\beta$ <sub>42</sub>, Gallyas silver impregnation (9) re-

<sup>1</sup>Division of Psychiatry Research, University of Zürich, August Forel Strasse 1, 8008 Zürich, Switzerland.  
<sup>2</sup>Experimental Genetics Group, Center for Human Genetics, K. U. Leuven, Campus Gasthuisberg, Leuven, Belgium.

\*These authors contributed equally to this work.

†To whom correspondence should be addressed at the Division of Psychiatry Research, University of Zürich, August Forel Strasse 1, 8008 Zürich, Switzerland. E-mail: goetz@bli.unizh.ch

‡To whom correspondence should be addressed at the Division of Psychiatry Research, University of Zürich, August Forel Strasse 1, 8008 Zürich, Switzerland. E-mail: nitsch@bli.unizh.ch